A Model for the Strength of Yarn-like Carbon Nanotube Fibers

Juan J. Vilatela, James A. Elliott, and Alan H. Windle*

Department of Materials Science and Metallurgy, University of Cambridge, Pembroke Street, Cambridge CB2 3QZ, United Kingdom

ABSTRACT A model for the strength of pure carbon nanotube (CNT) fibers is derived and parametrized using experimental data and computational simulations. The model points to the parameters of the subunits that must be optimized in order to produce improvements in the strength of the macroscopic CNT fiber, primarily nanotube length and shear strength between CNTs. Fractography analysis of the CNT fibers reveals a fibrous fracture surface and indicates that fiber strength originates from resistance to nanotube pull-out and is thus proportional to the nanotube−nanotube interface contact area and shear strength. The contact area between adjacent nanotubes is determined by their degree of polygonization or collapse, which in turn depends on their diameter and number of layers. We show that larger diameter tubes with fewer walls have a greater degree of contact, as determined by continuum elasticity theory, molecular mechanics, and image analysis of transmission electron micrographs. According to our model, the axial stress in the CNTs is built up by stress transfer between adjacent CNTs through shear and is thus proportional to CNT length, as supported by data in the literature for CNT fibers produced by different methods and research groups. Our CNT fibers have a yarn-like structure in that rather than being solid, they are made of a network of filament subunits. Indeed, the model is consistent with those developed for conventional yarn-like fibers.

KEYWORDS: carbon nanotube fiber · yarn · shear strength · polygonization · collapse · molecular mechanics

Even before the identification of carbon nanotubes (CNTs) as graphene layers rolled into cylinders with fullerene hemispheres as caps,[1] submicrometer diameter graphite filaments caught the attention of materials scientists due to their outstanding axial properties, which are closely related to those of graphite in the basal plane (see, for example, ref 2). In the case of CNTs, theoretical[3,4] and experimental work[5−7] indicates that their axial stiffness and strength are on the order of 1 TPa and 50 GPa, respectively, both in agreement with those for in-plane graphite[8] and graphene[9] (under the assumption that the cross section of the CNT is equal to that of the graphene layers in the tube). The interaction between layers in CNTs and between the tubes themselves is also similar to the interaction between graphene layers in graphite. It is mostly governed by weak van der Waals forces, which result in a low shear strength between adjacent graphene layers that facilitates CNTs sliding past each other and also for multiwall CNTs internally.[10]

The assembly of CNTs into a macroscopic fiber, with the tubes aligned parallel with respect both to each other and to the fiber axis, is a natural way of exploiting the axial properties of CNTs. This strategy is consistent with basic principles for making high-performance fibers, the properties of which are derived from extended molecules oriented along their main axis and parallel to the fiber.[11] Indeed, CNT fibers with tensile properties in the high-performance range are currently produced by various methods, and while their properties begin to match those of conventional fibers, such as aramid, they fall very short of the axial properties of their constituent CNTs. At present, there is a lack of studies that quantitatively relate the structure and composition of pure CNT fibers to their mechanical properties, and which therefore indicate the relative importance of the limiting factors affecting fiber strength.

This paper sets out to address this question by introducing a simple analytical model to calculate the theoretical axial strength of carbon CNT fibers based on the yarn-like character of the fiber and the fundamental mechanical properties of the constituent CNTs. Using data from both experiments and molecular mechanics calculations, the model aims to reconcile the tribological properties of graphite with the high CNT fiber strengths reported in the literature and suggests routes for further exploiting the axial strength and stiffness of CNTs in macroscopic fibers.

A Simple Fracture Model and Its Predictions. *The Model.* The starting point for the analysis is a simplified model for the fiber comprising a collection of parallel, rigid rods that can slide with respect to each other (analogous to a "bundle of pencils"), as shown in Figure 1a. Tensile stress is applied to either end of the fiber, resulting in failure when the fibrous elements have slid out of contact, at a stress assumed to be well below the

* Address correspondence to ahw1@cam.ac.uk.

Received for review October 28, 2010 and accepted February 4, 2011.

Published online February 24, 2011
10.1021/nn102925a

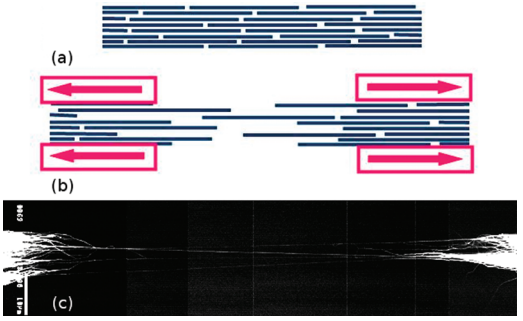

Figure 1. (a) Simple model of the fiber as collection of fibrous elements, (b) tensile fracture of fiber involving failure in shear between the fibrous elements, and (c) SEM micrograph of actual CNT fiber having undergone failure in tensile test (scale bar is 10 μm).

internal failure strength of the fibrous elements. The analysis of the tensile strength of the fiber is comparatively straightforward, and when this is done in terms of specific strength, σ', the result has a pleasing simplicity.

The simplified model for fracture shown in Figure 1b assumes that there is no correlation between the positions of the ends of the fibrous elements (which can be just single CNTs in the simplest embodiment), and that they are perfectly axially aligned and all of the same length and diameter. Determination of the failure strength of the fiber by shear between the elements, the mechanism envisaged in Figure 1b, requires an estimate of the total area of shear failure and the shear strength of the interfaces.

If we define a reference plane perpendicular to the axis which is at the center of the fracture, then each element will fail on the side of the fracture plane where it is shorter. Hence the mean length will be $L/4$, where L is the length of the element. The average surface area per tube will then be $2\pi rL/4$, but as the tubes are only in contact over a fraction of their circumference, this fraction being assigned the symbol Ω_2, the area of contact will be $N\Omega_2 2\pi rL/4$. Here, N is the number of tubes per cross section of the fiber and r the radius of the tubes assuming they are round. There is also another factor which needs to be taken into account, namely, that on average, only half of the tubes surrounding a given one will belong to the "other half" of the sample, and thus the contact area is reduced by another factor of 2, giving $N\Omega_2\pi rL/4$. If the interfacial fracture strength in shear is τ_F, the fracture load is $\tau_F N\Omega_2\pi rL/4$. If we now introduce Ω_1 as the fraction of graphene sheets on the outside of the CNT (or larger entity), the total mass of the tubes per unit length will be given by $N2\pi r\nu_G/\Omega_1$, this value being in kg m^{-1}, which will be tex (in g km^{-1}) $\times 10^{-6}$. Hence the specific strength in N tex^{-1} will be given by

$$\sigma' = \frac{1}{\nu_G}\Omega_1\Omega_2\tau_F\frac{L}{8}\times 10^6 \qquad (1)$$

where σ' is the specific stress in N tex^{-1} (GPa/SG); Ω_1 is the fraction of the total number of graphene layers that are on the outside of the fibrous element, such as a CNT (for single-wall CNT $\Omega_1 = 1$, double-wall CNT = ~0.5, multiwall CNT < 0.5, bundle of say 50 double-wall CNTs < 0.1); Ω_2 is the fraction of the surface of the outer graphene wall(s) of the element in contact with neighboring elements; τ_F is the interfacial shear strength in Pa (the surface energy of the CNT, γ, has a negligible effect on strength for the length of fibrous elements and the range of inter element shear strengths under consideration); L is the mean length of the fibrous elements; ν_G is the areal density of a single graphene sheet, which is 0.75×10^{-6} kg m^{-2}.

Substituting the value for ν_G, the relation simplifies further to

$$\sigma' = \frac{1}{6}\Omega_1\Omega_2\tau_F L \qquad (2)$$

with the numerical prefactor of 1/6 having the units of m^2 kg^{-1}.

Equation 2, while having a pleasing simplicity as a result of using specific stress, is consistent with accepted theories on the strength of yarns, which take yarn strength to be proportional to the length of the staple fiber, the coefficient of static friction between staples, and the surface area of contact between them.[12,13]

Figure 1c illustrates the fracture process observed in the fiber. It suggests that the fibrous elements involved will be bundles of carbon nanotubes, which make up the fibrous structure observable at the resolution of the micrograph. In order to calculate a value for the specific stress, we must now consider reasonable values for the parameters Ω_1, Ω_2, τ_F, and L.

Values for Ω_1 and Ω_2. In the case of individual CNTs, Ω_1 is approximately $1/N$, where N is the number of graphene layers in the tube; thus, if we are to assume a large diameter double-wall CNT as the basic fibrous element, then this value will be ~0.5. If the basic elements responsible for stress transfer in the fiber were in fact bundles of CNTs, then Ω_1 would be considerably decreased as only the tubes in the perimeter of the bundle would contribute to the transfer of stress by shear.

When a bundle of SWNTs forming a hexagonal array is considered, as shown in Figure 2a, and the number of tubes on a side of the hexagon is defined as l, the ratio of CNTs on the perimeter of the array divided by the total number of tubes is

$$\frac{6(l-1)}{3l^2 - l + 1} \qquad (3)$$

If one was to assume that the element failing in shear in a CNT fiber is a bundle, then the ratio above multiplied by the reciprocal of the number of layers would effectively give the value of Ω_1. In this scenario, Ω_1 decreases rapidly with increasing bundle size and takes a value of less than 0.2 for relatively small bundles of a few tens of nanometers (Figure 2b).

The model would also be appropriate for estimating the strength of the bundles themselves, with the basic

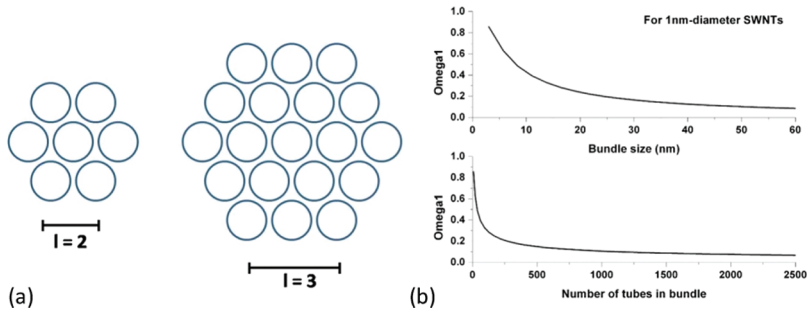

Figure 2. (a) Schematic of a bundle of hexagonally packed SWNTs, (b) plot of the ratio of tubes on the perimeter over the total number of tubes against bundle size [$\sim 2(l-1)$] and total number of tubes [$3l^2 - l + 1$].

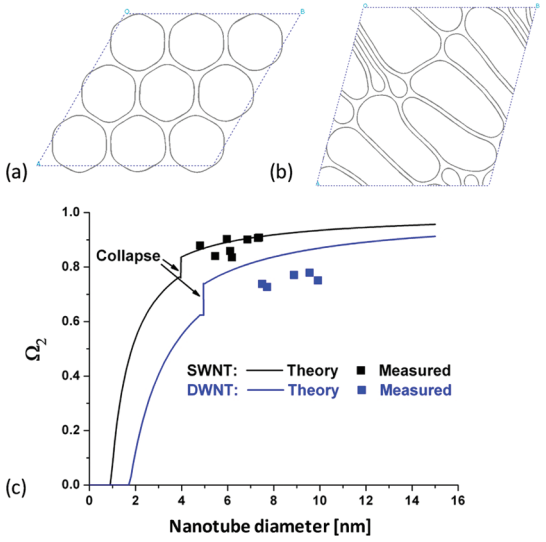

Figure 3. (a) Polygonized cross section of (30,30) SWNT bundle (tube diameter 4.08 nm) with $\Omega_2 = 0.75$, (b) collapsed cross section of (50,50) SWNT bundle (tube diameter 6.80 nm) with $\Omega_2 = 0.95$, and (c) comparison of theoretical (see Supporting Information) and experimental values of Ω_2 for SWNT and MWNT against CNT diameter. Experimental values are determined by image analysis of the HRTEM micrographs in refs 16 (reproduced in Figure 4a) and 17.

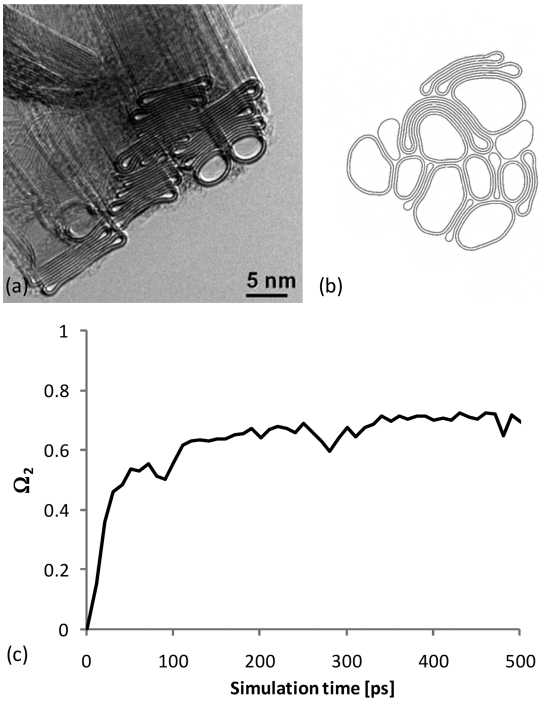

Figure 4. (a) TEM micrograph of collapsed bundle, (b) MD simulation of equivalent bundle after 0.5 ns, and (c) plot of Ω_2 *versus* time for the equivalent bundle simulated using molecular dynamics at constant volume and temperature (300 K).

fibrous element now being the nanotube and Ω_2 being the fraction of the outside surface of the individual nanotube which is in contact with its neighbor. The most straightforward factor affecting Ω_2 is that of "polygonization" (Figure 3a), whereby neighboring tubes flatten themselves against each other and gain bonding area at the expense of an increase in curvature energy.[14] The fraction of perimeter in contact with neighboring tubes (Ω_2) can be derived using classical elasticity theory (see Supporting Information). The other aspect which is relevant here is the self-collapse of the CNTs (Figure 3b), which is observed for relative large diameter tubes with thin walls.[15] It is a feature of the CNTs in the CNT fiber under consideration,[16] and it implies that higher Ω_2 values can be achieved from completely flattened tubes due to the additional graphene−graphene contact across the cores of the tubes.

Figure 3c presents a plot of predicted values of Ω_2 against CNT diameter, assuming $e = 1$ and $\alpha = 2$ (as defined in Supporting Information, Figure S1), and taking $\gamma = 0.13\ \mathrm{J\,m^{-2}}$ and the flexural bending modulus $D = 2.21 \times 10^{-19}$ J. The graph includes the prediction for polygonized and collapsed tubes of 1 and 2 layers and experimental values obtained by image analysis of high-resolution electron micrographs of bundles of CNTs (Figure 2 in ref 16 and Figure S3-A in ref 17). The graph shows clearly the increase in contact between tubes as they polygonize and ultimately collapse into ribbons, as favored by a large tube diameter a small number of layers.

In reality, the geometry of nanotubes in the CNT fiber is much more complex than those shown in Figure 3a,b and will involve a distribution of diameters and number of walls. Figure 4a shows a cross section of a

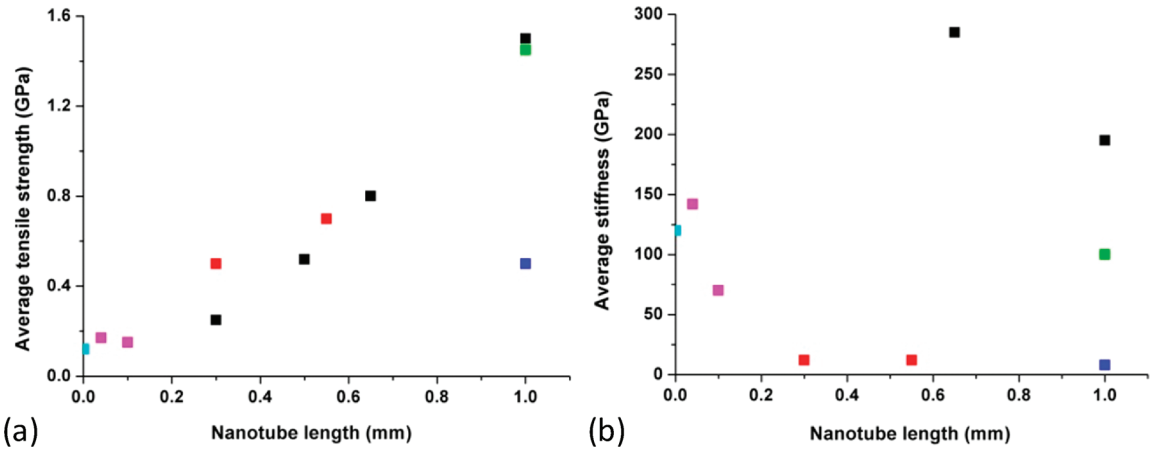

Figure 5. Reported values of (a) fiber strength and (b) stiffness of fibers made of CNTs of different lengths and number of layers. The data are for fibers spun from arrays of aligned CNTs (black, DWNTs and MWNTs;[18] red, MWNTs;[21] and blue, MWNTs[22]), directly from the gas phase (green, mostly DWNTs[17]) and from a liquid crystal dispersion (pink, MWNTs;[23] and light blue, SWNTs[24]).

TABLE 1. Shear Strengths of Graphite and CNTs

material	method	shear strength (MPa)	reference
single crystal graphite	mechanical shear	0.029	25
MWNT on graphite	tube rolling and sliding	2.0	26
MWNTs	intratube sliding	0.08	27
MWNTs	intratube sliding	0.04<	28
SWNTs and MWNTs	intratube sliding	4.0	29
MWTNs	intratube sliding	2.0−69.0	30
bundle of SWNTs	molecular mechanics and molecular dynamics	0.9	31
bundle of SWNTs	molecular dynamics	36	32
bundle of SWNTs	molecular dynamics	0.1−6.1	33
bundle of SWNTs	molecular dynamics	∼5	34

CNT bundle, taken from Figure 2 in ref 16 (bottom), in which there is a mixture of predominantly double-wall CNTs with an average external diameter of 6.6 nm. The larger diameter tubes near the center of the bundle have collapsed, whereas the smaller diameter tubes near edge are still inflated, in agreement with Figure 3c and theory presented in Supporting Information. A model of this bundle is built from armchair tubes with inter tube radii differing by the layer spacing in turbostratic graphite and by taking measured external diameters of CNTs from Figure 4a. The resulting structure after 0.5 ns of molecular dynamics simulation at 300 K is shown in Figure 4b. Similarly to the experimental observation, most of the tubes in the bundle have collapsed. For reference, the value of Ω_2 is plotted as function of time in Figure 4c starting from the completely uncollapsed state, $\Omega_2 = 0$. Although the collapse of the simulated bundle is not as complete, the coupling of modeling and experimental information would suggest a value for Ω_2 of the CNTs in our fiber in the range of 0.7−0.85.

Length of the Fibrous Elements, L. The length of the CNTs in the fibers has been measured to be on the order of 1 mm,[17] which would correspond to an axial ratio of ∼10^5. The importance of length of the component fibrous elements of a yarn has been recognized for a long time and its relevance to CNT fibers recently noted.[18,19]

For comparison with the theoretical prediction, a summary of the values of fiber strength reported in the literature for various CNT fibers, where the average length of the CNTs is also reported, is presented in Figure 5 as a plot of fiber strength against CNT length. Values of fiber strength in units of GPa rather than GPa/SG are plotted because not all values of fiber SG are reported. In spite of the fact that the type of CNTs vary (covering the range SWNT to MWNT), the plot shows a clear correlation between fiber strength and CNT length. Note that the same correlation is not present for the fiber stiffness. This suggests that the stiffness of the CNT fibers reflects mostly differences in the quality of orientation of CNTs in the fibers,[20] in some cases due to specific processing parameters such as the application of twist.

Shear Strength between Graphene Layers, τ_F. The shear stress which can be transmitted between adjacent graphene layers has been measured by a variety of techniques, ranging from classical measurements on graphite single crystals[25] to various sliding geometries in the AFM.[26−30] It has also been estimated by simulations of the sliding of two adjacent graphene layers, either as a CNT

pulled out from a bundle[31−33] or as an inner layer pulled out of a MWNT.[34,35] Some data are summarized in Table 1.

The range of experimental values is wide, from 0.04 to 69.0 MPa. The scatter is unlikely to be entirely due to conditions in the experimental environment[36] as measurements in vacuum give values that range from 0.04[28] to 69 MPa.[30] In a recent experiment by Suekane *et al.*,[30] two parallel CNTs overlapped by a few micrometers were pulled apart longitudinally measuring load against displacement. There was a friction stress of 40 MPa with as-synthesized tubes, but this decreased below the detection limit of 2 MPa for CNTs that had been cleaned by annealing. Other experiments involving larger contact areas, including graphite crystals, yield values in the range of 0.015−0.085 MPa for "clean" graphite surfaces.[25] The experimental work would suggest a value for τ_F of 0.05 MPa (within the lower range of literature values), as our CNTs within the bundles show no evidence of surface contamination.

Extracting a shear strength value from the modeling work is rather more complicated. The results suggest that the concept of shear strength cannot be easily extended to two perfect graphene layers, and that the tribological properties of these two theoretical surfaces depend largely on their crystallographic registry, spacing, and constraints on them.[34] Thus, the values of shear strength from modeling also cover a broad range from 0.1 to 36 MPa,[33,32,31] and furthermore, some reports suggest that in bundles of incommensurate tubes the frictional force when displacing the tubes does not scale with overlapping length,[34,35] making the concept of shear strength for that interface ambiguous. For these reasons, we keep the estimate of 0.05 MPa for clean graphene surfaces with turbostratic spacing.

In our case, the self-diffusion coefficients calculated for longitudinal mean-squared displacement parallel to the nanotube axis for tubes in the bundle shown in Figure 4b are in the range of 1 to 400 $\times$ 10^{-10} m^2 s^{-1}, which is consistent with a very low value of shear strength. Although obtaining an accurate estimate of shear strength from molecular simulations would require much longer lengths of nanotube together with the introduction of defects, we have shown here that even perfect CNTs with uniform chiral angle can slide relatively easily with respect to each other parallel to the bundle axis. In reality, our CNT fiber is composed of a wide variety of nonperfect CNTs separated by a distance close to that in turbostratic graphite, and thus the value for τ_F of 0.05 MPa at the lower end of the range seems reasonable.

It is also noteworthy that the force required to slide two graphene surfaces past each other has in fact two components, one arising from the creation of the new surface and the other from the interlayer "friction". This poses a problem when dealing with short graphene layers or CNTs—as is the case in experiments involving CNT pullout using an AFM and can be in the modeling work—since the first component is several orders of magnitude higher than the second one. It is therefore very challenging to obtain both components—either experimentally or though simulations—simultaneously and is probably part of the reason why both modeling and experimental work give such a broad range of shear strength values. However, for CNTs 1 mm long, such as those in CNT fibers spun from the gas phase, the ratio of the contributions will be

$$\frac{\frac{L}{4} \times \tau_F}{\gamma} \sim 100 \qquad (4)$$

and thus the contribution of the surface energy can be neglected.

Prediction of Bundle Strength. Substituting the estimated values as follows: $\Omega_1 = 0.5$, $\Omega_2 = 0.85$, $\tau_F = 0.05 \times 10^6$ Pa, and $L = 10^{-3}$ m, into eq 2, the prediction of tensile strength is 3.54 N tex^{-1}, a value much closer to the range of values reported for CNT fiber than to the theoretical strength of a graphene layer. This value could be taken as an estimate of the strength of our carbon CNT bundles, although the question moves on to what is the strength of the bundle network itself. Another aspect to consider is the likelihood that sufficient stress is transferred in shear to actually fracture some of the 1 mm long CNTs in tension. The most severe case would be for a CNT embedded equally on either side of the fracture plane and, unusually, completely surrounded by CNTs from which it is pulling out. In this case, the maximum force on the CNT will be $\Omega_1\Omega_2 2\pi r\tau_F L/2$, so for the outer layer, if we assume it carries all of the load, the force per unit circumference of the graphene outer layer will be $\Omega_2\tau_F(L/2)$ = 21 N m^{-1}, significantly less than the 42 N m^{-1} measured strength for a single layer.[9] It is therefore unlikely that many, if any, carbon CNTs will themselves break in tension as the fiber itself fractures.

Network of Bundles and Strength of Fiber. The fractured ends of a fiber (Figure 1c) show fibrous elements which are not individual CNTs but bundles of perhaps 50−100 such tubes. In the region of the fracture, the bundles have pulled out from each other, suggesting that the strength is limited by the coherence of this network more than the strength of individual bundles. Fractography analysis of CNT fibers gives no indication whatsoever of the natural termination of any bundles in the opened up structure near to the fracture itself (Figure S2, Supporting Information). Indeed, the bundle network appears continuous, with the nodes corresponding to the sharing of CNTs between the different segments of the bundle network. It is also significant in this respect that the apparent fractured fiber in Figure 1c still has a few bundles connecting both ends. It is clear that some of the bundles, at least, are quasi-continuous, and the fracture involves a degree of unraveling of the entangled bundle network.

In their paper, Koziol *et al.*[17] showed that when fibers were tested at short gauge lengths (~1 mm) the

strength and stiffness distributions showed a bimodal distribution, there being a peak between 1 and 1.5 N tex^{-1}, which corresponded to the strength of much longer samples, the *extrinsic* peak, and a second peak in the region of 5 N tex^{-1}. The shorter the gauge length, the more intense the second, *intrinsic*, peak in the distribution, that is, the higher the probability of seeing a stronger sample. We propose that the extrinsic strength shown by longer lengths of the material corresponds to the resistance of the bundle network to failure in shear, which also involves unraveling of the network, while the higher peak strength at short gauge lengths corresponds to the case where the majority of bundles span from one grip to the other, and thus this strength/stiffness measurement at short gauge length corresponds to the property of the bundles themselves. One can appreciate this from Figure 1c, where some of the bundles which are pulling out without breaking are a significant fraction of a millimeter long.

The predicted strength given by the model, when it is parametrized in terms of the individual nanotubes being the basic fibrous elements, is thus that corresponding to the strength of the bundles. The model value of 3.5 N tex^{-1} must be compared with the observed *intrinsic* strength of 5 N tex^{-1}. Either of these values is at or above the upper end of the strength of currently available high-performance fibers and thus should be seen as highly desirable. The model also clearly indicates those parameters which can be optimized to still further enhance the bundle strength, those in the product $\Omega_1\Omega_2\tau_F L$ (eq 2).

A high value of $\Omega_1\Omega_2$ is dependent on the nature of the carbon CNTs, and it is likely that large diameter, thin wall tubes which autocollapse are ideal in this respect. The maximization of τ_F is a clear opportunity to increase the strength, and work in hand is addressing this factor specifically. It is also possible that covalent cross-linking of the bundles may increase the bundle strength, which currently appears to be the limiting factor. The CNTs formed in the process are unusually long (~1 mm) by most standards and particularly so for the floating catalyst method. Careful control of the many interacting process variables may help to increase this, but the length will probably be limited by the physical dimensions of the CNT cloud formed at the point of reaction.

The strength of the entangled network of bundles does, however, present the next modeling challenge. While the greater mass per unit surface area of a bundle compared with an individual nanotube leads to a prediction of a considerably lower strength through a lower Ω_2, one also needs to take into account that the mutual alignment of the bundles is not as perfect of that of the nanotubes within the bundles, leading to a reduced value of Ω_1. On the other hand, there may also be a contribution to network strength from the entanglements themselves, which is difficult to assess in quantitative terms. Techniques for the enhancement of interbundle strength are under development and will be reported soon.

CONCLUSIONS

A model has been developed for the strength of yarn-like carbon nanotube fibers. The structure of the fiber appears to be hierarchical, with nanotubes self-assembling into bundles and the bundles forming an aligned network in the fiber. The model leads to a relation for the specific strength in terms of the characteristics of the basic fibrous elements, their surface area per unit mass, their contact area with neighbors, their length, and the strength of the interface between them in shear. In the case where the basic fibrous element is the nanotube, the estimated strength of 3.5 N tex^{-1} will be that of the bundle. On the other hand, the strength of the fiber will also depend on the strength of the network of bundles, a figure which is much more difficult to estimate, as values will be needed for interbundle contact area, effective length of the bundles, and the resistance of network points to sliding. Nevertheless, the model provides a basis for discriminating between intrinsic fiber strength, measured on short gauge length samples at ~5 N tex^{-1}, which corresponds to bundle strength, and extrinsic strength, a lower value seen (1−2 N tex^{-1}) in all longer samples, which is probably related to the coherency of the network of bundles and its stability under stress.

Overall, the model provides a rationale for further improvements in fiber properties, both through more precise process control and the possibility of post-processing operations to enhance the shear strength of the intergraphene interfaces.

MATERIALS AND METHODS

The fibers in Figures 1b and S2 (Supporting Information) were made by direct spinning of a CNT aerogel from the gas phase during CNT growth by chemical vapor deposition (CVD).[37] Fractography images were obtained from *in situ* testing using a Deben microtest tensile stage in a JEOL 820 SEM and from *ex situ* analysis of fracture surfaces using a JEOL 6340F FEGSEM.

The molecular dynamics calculations shown in Figures 3a,b and 4b were carried out using the DL_POLY package[38,39] (version 2.20) from Daresbury Laboratory. The constant stress ensemble (at zero pressure and 300 K) was used in Figure 3a,b, and the canonical ensemble (at fixed total volume and 300 K) was used in Figure 4b. Simulations were carried out using periodic boundary conditions (with cell dimension parallel to CNT axis 2.45 nm), a time step of 1 fs, and a Nosé−Hoover thermostat with relaxation time of 10 ps. The force field was based on a modified version of DREIDING, as used by Elliott *et al.*[40] in an earlier study of CNT collapse. All CNTs in Figure 4b were assumed to be of the armchair type.

Acknowledgment. The authors wish to acknowledge the U.S. Army International Technology Center London, CONACYT

Mexico, and the EPSRC for funding. They would also like to acknowledge the support of Accelrys Inc. for providing modelling software (Materials Studio) used for the molecular simulations.

Supporting Information Available: Derivation is given of Ω_2, the fraction of the surface of the outer graphene wall(s) of the load-bearing element in contact with its neighbors in the fiber, which was used to generated the curves in Figure 3c. Figure S1 shows a schematic of bundles of (a) polygonized and (b) collapsed CNTs with different fractions of their perimeter in contact. Figure S2 shows a SEM micrograph of the fracture surface of a CNT fiber. This material is available free of charge *via* the Internet at http://pubs.acs.org.

REFERENCES AND NOTES

1. Iijima, S. Helical Microtubules of Graphtic Carbon. *Nature* **1991,** *354*, 56–58.
2. Dresselhaus, M. S.; Dresselhaus, G.; Sugihara, K.; Spain, I. L.; Goldberg, H. A. *Graphite Fibers and Filaments*; Springer-Verlag: Berlin, 1988.
3. Lu, J. Elastic Properties of Carbon Nanotubes and Nanoropes. *Phys. Rev. Lett.* **1997,** *79*, 1297–1300.
4. Yakobson, B. I.; Brabec, C. J.; Bernholc, J. Nanomechanics of Carbon Tubes: Instabilities beyond Linear Response. *Phys. Rev. Lett.* **1996,** *76*, 2511–2514.
5. Wong, E. W.; Sheehan, P. E.; Lieber, C. M. Nanobeam Mechanics: Elasticity, Strength, and Toughness of Nanorods and Nanotubes. *Science* **1997,** *277*, 1971–1975.
6. Walters, D. A.; Ericson, L. M.; Casavant, M. J.; Liu, J.; Colbert, D. T.; Smith, K. A.; Smalley, R. E. Elastic Strain of Freely Suspended Single-Wall Carbon Nanotube Ropes. *Appl. Phys. Lett.* **1999,** *74*, 3803–3805.
7. Yu, M.-F.; Lourie, O.; Dyer, M. J.; Moloni, K.; Kelly, T. F.; Ruoff, R. S. Strength and Breaking Mechanism of Multiwalled Carbon Nanotubes under Tensile Load. *Science* **2000,** *287*, 637–640.
8. Kelly, A. *Strong Solids*; Oxford University Press: Oxford, 1966.
9. Lee, C.; Wei, X.; Kysar, J. W.; Hone, J. Measurement of the Elastic Properties and Intrinsic Strength of Monolayer Graphene. *Science* **2008,** *321*, 385–388.
10. Saito, R.; Matsuo, R.; Kimura, T.; Dresselhaus, G.; Dresselhaus, M. Anomalous Potential Barrier of Double-Wall Carbon Nanotube. *Chem. Phys. Lett.* **2001,** *348*, 187–193.
11. Staudinger, H. *Die Hochmolekularen Organischen Verbindungen*; Springer-Verlag: Berlin, 1932.
12. Gregory, J. Cotton Yarn Structure Part IV—The Strength of Twisted Yarn Elements in Relation to the Properties of the Constituent Fibres. *J. Text. Inst.* **1954,** *44*, T499–T514.
13. Morlier, O.; Orr, R.; Grant, J. The Relation of Length to Other Physical Properties of Cotton Fibers. *Text. Res. J.* **1951,** *21*, 6–13.
14. Ruoff, R. S.; Tersoff, R. S.; Lorents, D. C.; Subramoney, S.; Chan, B. Radial Deformation of Carbon Nanotubes by van der Waals Forces. *Nature* **1993,** *364*, 514–516.
15. Chopra, N. G.; Benedict, L. X.; Crespi, V. H.; Cohen, M. L.; Louie, S. G.; Zettl, A. Fully Collapsed Carbon Nanotubes. *Nature* **1995,** *377*, 135–138.
16. Motta, M.; Moisala, A.; Kinloch, I. A.; Windle, A. H. High Performance Fibres from "Dog Bone" Carbon Nanotubes. *Adv. Mater.* **2007,** *19*, 3721–3726.
17. Koziol, K.; Vilatela, J.; Moisala, A.; Motta, M.; Cunniff, P.; Sennett, M.; Windle, A. High-Performance Carbon Fiber. *Science* **2007,** *318*, 1892–1895.
18. Zhang, X.; Li, Q.; Holesinger, T. G.; Arendt, P. N.; Huang, J.; Kirven, P. D.; Clapp, T. G.; DePaula, R. F.; Liao, X.; Zhao, Y.; *et al.* Ultrastrong, Stiff, and Lightweight Carbon-Nanotube Fibers. *Adv. Mater.* **2007,** *19*, 4198–4201.
19. Behabtu, N.; Green, M.; Pasquali, M. Carbon Nanotube-Based Neat Fibers. *Nano Today* **2008,** *3*, 24–34.
20. Liu, T.; Kumar, S. Effect of Orientation on the Modulus of SWNT Films and Fibers. *Nano Lett.* **2003,** *3*, 647–650.
21. Atkinson, K. R.; Hawkins, S. C.; Huynh, C.; Skourtis, C.; Dai, J.; Zhang, M.; Fang, S.; Zakhidov, A. A.; Lee, S. B.; Aliev, A. E.; *et al.* Multifunctional Carbon Nanotube Yarns and Transparent Sheets: Fabrication, Properties, and Applications. *Physica B* **2007,** *394*, 339–343.
22. Zhang, S.; Zhu, L.; Minus, M. L.; Chae, H. G.; Jagannathan, S.; Wong, C.-P.; Kowalik, J.; Roberson, L. B.; Kumar, S. Solid-State Spun Fibers and Yarns from 1-mm Long Carbon Nanotube Forests Synthesized by Water-Assisted Chemical Vapor Deposition. *J. Mater. Sci.* **2008,** *43*, 4356–4362.
23. Zhang, S.; Koziol, K. K.; Kinloch, I. A.; Windle, A. H. Macroscopic Fibers of Well-Aligned Carbon Nanotubes by Wet Spinning. *Small* **2008,** *4*, 1217–1222.
24. Ericson, L. M.; Fan, H.; Peng, H.; Davis, V. A.; Zhou, W.; Sulpizio, J.; Wang, Y.; Booker, R.; Vavro, J.; Guthy, C.; *et al.* Macroscopic, Neat, Single-Walled Carbon Nanotube Fibers. *Science* **2004,** *305*, 1447–1450.
25. Soule, D. E.; Nezbeda, C. W. Direct Basal-Plane Shear in Single-Crystal Graphite. *J. Appl. Phys.* **1968,** *39*, 5122–5129.
26. Falvo, M. R.; Taylor, R. M.; Helser, A.; Chi, V.; Brooks, F. P., Jr; Washburn, S.; Superfine, R. Nanometre-Scale Rolling and Sliding of Carbon Nanotubes. *Nature* **1999,** *397*, 236–238.
27. Yu, M.; Yakobson, B. I.; Ruoff, R. S. Controlled Sliding and Pullout of Nested Shells in Individual Multiwalled Carbon Nanotubes. *J. Phys. Chem.* **2000,** *104*, 8764–8767.
28. Kis, A.; Jensen, K.; Aloni, S.; Mickelson, W.; Zettl, A. Interlayer Forces and Ultralow Sliding Friction in Multiwalled Carbon Nanotubes. *Phys. Rev. Lett.* **2006,** *97*, 025501.
29. Bhushan, B.; Ling, X.; Jungen, A.; Hierold, C. Adhesion and Friction of a Multiwalled Carbon Nanotube Sliding against Single-Salled Carbon Nanotube. *Phys. Rev. B* **2008,** *77*, 165428.
30. Suekane, O.; Nagataki, A.; Mori, H.; Nakayama, Y. Static Friction Force of Carbon Nanotube Surfaces. *Appl. Phys. Exp.* **2008,** *1*, 064001.
31. Qian, D.; Liu, W. K.; Ruoff, R. S. Load Transfer Mechanism in Carbon Nanotube Ropes. *Compos. Sci. Technol.* **2003,** *63*, 1561–1569.
32. Cornwell, C. F.; Majure, D.; Haskins, R.; Lee, N. J.; Ebeling, R.; Maier, R.; Marsh, C.; Bednar, A.; Kirgan, R.; Welch, C. R. Critical Carbon Nanotube Length in Fibers. *DoD HPCMP Users Group Conference*, 2008; pp 180—186.
33. Zhang, X.; Li, Q. Enhancement of Friciton between Carbon Nanotubes: An Efficient Strategy To Strengthen Fibers. *ACS Nano* **2010,** *4*, 312–316.
34. Kolmogorov, A. N.; Crespi, V. H. Smoothest Bearings: Interlayer Sliding in Multiwalled Carbon Nanotubes. *Phys. Rev. Lett.* **2000,** *85*, 4727–4730.
35. Xia, Z.; Curtin, A. Pullout Forces and Friction in Mutiwall Carbon Nanotubes. *Phys. Rev. B* **2004,** *69*, 233408.
36. Lancaster, J. K.; Pritchard, J. R. The Influence of Environment and Pressure on the Transition to Dusting Wear of Graphite. *J. Phys. D: Appl. Phys.* **1981,** *14*, 747–762.
37. Li, Y. L.; Kinloch, I. A.; Windle, A. H. Direct Spinning of Carbon Nanotube Fibers from Chemical Vapor Deposition Synthesis. *Science* **2004,** *304*, 276–278.
38. Smith, W.; Forester, T. R. DL_POLY_2.0: A General-Purpose Parallel Molecular Dynamics Simulation Package. *J. Mol. Graph.* **1996,** *14*, 136–141.
39. Smith, W.; Yong, C. W.; Rodger, P. M. DL_POLY: Application to Molecular Simulation. *Mol. Simul.* **2002,** *28*, 385–471.
40. Elliott, J. A.; Sandler, J. K.; Windle, A. H.; Young, R. J.; Shaffer, M. S. Collapse of Single-Wall Carbon Nanotubes Is Diameter Depenent. *Phys. Rev. Lett.* **2004,** *92*, 095501.